

# Spectroscopic and laser characteristics of Ti:Al<sub>2</sub>O<sub>3</sub>

P. F. Moulton

Schwartz Electro-Optics, Inc., 45 Winthrop Street, Concord, Massachusetts 01742

Received July 15, 1985; accepted October 4, 1985

Spectroscopic measurements and laser performance of Ti:Al<sub>2</sub>O<sub>3</sub> are discussed in detail. Data on absorption and fluorescence spectra and fluorescence lifetime as a function of temperature are presented. Laser characteristics observed with pulsed-dye-laser, frequency-doubled Nd:YAG-laser, and argon-ion-laser pumping are covered and show that nearly quantum-limited conversion of pump radiation can be achieved, along with tuning over the wavelength range 660–986 nm.

## INTRODUCTION

The Ti:Al<sub>2</sub>O<sub>3</sub> solid-state laser is one of the more recently demonstrated<sup>1</sup> tunable systems and the first to use Ti<sup>3+</sup> as the active ion. As will be discussed below, the Ti:Al<sub>2</sub>O<sub>3</sub> laser is characterized by a simple energy-level structure, a broad tuning range, and a relatively large gain cross section. This paper will cover basic spectroscopy of Ti:Al<sub>2</sub>O<sub>3</sub> and properties of laser operation under both pulsed and quasi-cw excitation.

## SPECTROSCOPY

The electronic structure of the Ti<sup>3+</sup> ion is a closed shell plus a single 3*d* electron. The free-space, fivefold-degenerate (neglecting spin) *d*-electron levels are split by the crystal field of the host. In the host Al<sub>2</sub>O<sub>3</sub> the site for the Ti<sup>3+</sup> ion has trigonal symmetry; the crystal field can be viewed as the sum of cubic- and trigonal-symmetry components. The cubic field dominates and splits the Ti<sup>3+</sup> energy levels into a triply degenerate <sup>2</sup>T<sub>2</sub> ground state and a doubly degenerate <sup>2</sup>E excited state. The trigonal field splits the ground <sup>2</sup>T<sub>2</sub> state into two levels, and the lower of the two levels is split further into two levels by the spin-orbit interaction.<sup>2</sup> The energy differences between the lowest-energy <sup>2</sup>T<sub>2</sub> level and the other <sup>2</sup>T<sub>2</sub> levels have been determined by infrared absorption measurements<sup>2,3</sup> to be 38 and 107 cm<sup>-1</sup>; the dynamic Jahn-Teller effect has been shown to play a major role in determining those energies.<sup>4</sup>

The separation between the <sup>2</sup>T<sub>2</sub> and <sup>2</sup>E states was first determined by McClure<sup>5</sup> through optical absorption measurements to be around 19 000 cm<sup>-1</sup>, as evidenced by an absorption band in the visible wavelength region. Later measurements<sup>6,7</sup> confirmed that the band observed was, in fact, due to the Ti<sup>3+</sup> ion. Figure 1 shows our measurement, for two polarizations at room temperature, of the <sup>2</sup>T<sub>2</sub> → <sup>2</sup>E absorption band. The double-peaked nature of the band is due to the Jahn-Teller splitting of the <sup>2</sup>E state. McClure<sup>5</sup> measured the peak splitting to be 1850 cm<sup>-1</sup> at a crystal temperature of 77 K, and Eigenmann<sup>8</sup> later showed that two Gaussian bands with centers of 20 476 and 17 987 cm<sup>-1</sup> and linewidths of 1295 and 921 cm<sup>-1</sup>, respectively, were good approximations to the 77-K band shape. The cross-section scale shown in Fig. 1 was derived from measurements on a sample with a Ti concentration of 3.3 × 10<sup>19</sup> cm<sup>-3</sup> (or ~0.1

wt. % Ti<sub>2</sub>O<sub>3</sub> in Al<sub>2</sub>O<sub>3</sub>) as determined by x-ray fluorescence techniques. All concentrations discussed in this paper refer to those in the crystal, based on the cross-section data. Since the x-ray measurement does not discriminate between different valence states of the Ti ion, it may be that not all the ions were Ti<sup>3+</sup>, and thus the cross section represents a lower bound.

Data on fluorescence from the <sup>2</sup>E → <sup>2</sup>T<sub>2</sub> transition of Ti:Al<sub>2</sub>O<sub>3</sub> was first reported by Gachter and Koningstein,<sup>9</sup> who associated a number of low-temperature details in the spectra with zero-, one- and two-phonon transitions. In particular, they established that the highest-energy zero-phonon line was at 16 216 cm<sup>-1</sup>. Our measurements of the polarized fluorescence spectra at 300 K (Fig. 2) show emission peaking at and extending to longer wavelengths than that in Ref. 9; our results<sup>10</sup> agree with the behavior of the Ti:Al<sub>2</sub>O<sub>3</sub> laser systems discussed below.

We observed the fluorescence decay at room temperature to be exponential, with a lifetime of 3.15 ± 0.05 μsec. The lifetime measurement was accomplished by recording (on a transient digitizer) the detected broadband fluorescence decay from samples excited at 490 nm by a pulsed dye laser. Six different samples grown by three different techniques and having concentrations ranging from <0.01 to 0.1 wt. % Ti<sub>2</sub>O<sub>3</sub> were examined and showed the same decay time within the error limits given. Figure 3 plots the variation in lifetime with temperature for one sample doped at the 0.1% level. Some of the reduction in lifetime with increasing temperature could be associated with an increased phonon-induced radiative transition rate, but the rapid reduction in lifetime at high temperatures is characteristic of fluorescence quenching due to multiphonon nonradiative decay.<sup>11</sup>

The only other short-wavelength absorption associated with the Ti<sup>3+</sup> ion in Al<sub>2</sub>O<sub>3</sub> is a charge-transfer band, produced by the transition in which an electron on one of the oxygen ions moves to the Ti-ion site, changing the ion state to Ti<sup>2+</sup>. Tippins<sup>12</sup> measured charge-transfer bands for a number of transition-metal ions in Al<sub>2</sub>O<sub>3</sub> and reported the existence of the Ti<sup>3+</sup> charge-transfer band peaking around 180 nm. Our measurements, done on a 0.1-mm-thick sample containing ~0.05 wt. % Ti<sub>2</sub>O<sub>3</sub>, show almost exactly the same spectral shape observed by Tippins up to the short-wavelength limit (190 nm) of the spectrophotometer used and include evidence of the small peak at 260 nm attributed by Tippins to Fe<sup>3+</sup> impurities. However, the extinction

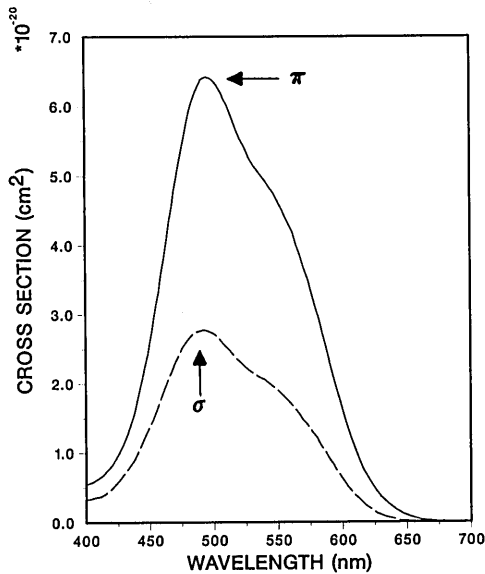


Fig. 1. Polarized absorption cross sections for the  ${}^2T_2 \rightarrow {}^2E$  transition in  $\text{Ti:Al}_2\text{O}_3$ . Baseline was arbitrarily set to zero for both polarizations at 700 nm.

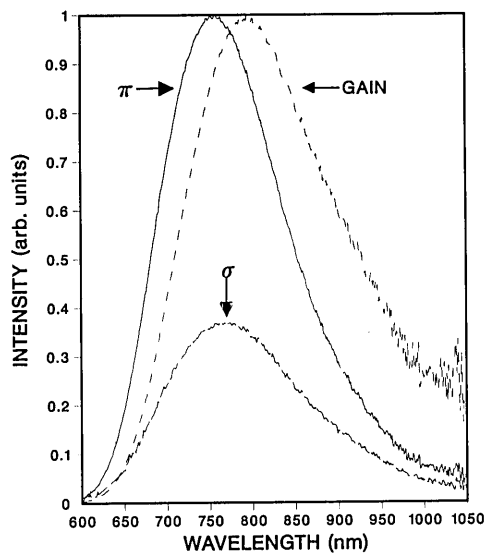


Fig. 2. Polarized fluorescence spectra and calculated gain line shape for  $\text{Ti:Al}_2\text{O}_3$ .

coefficient of our measured absorption,  $27 \text{ cm}^{-1}$  at 190 nm, is considerably less than the value of  $\sim 180 \text{ cm}^{-1}$  deduced from Tippins data, which is surprising, since the crystal examined by Tippins had an estimated doping level smaller than our sample by more than an order of magnitude. Tippins noted that an *a priori* calculation of the charge-transfer band positions in  $\text{Al}_2\text{O}_3$  for four ions other than  $\text{Ti}^{3+}$  gave good agreement with data, while the band observed in the  $\text{Ti}^{3+}$ -doped sample was 1 eV lower in energy than predicted. It was also noted that the  $\text{Ti}^{3+}$  band, because of the closeness of ionization potentials between  $\text{Ti}^{2+}$  and  $\text{Al}^{2+}$ , might be close to the intrinsic absorption edge of  $\text{Al}_2\text{O}_3$  and therefore difficult to observe. We conclude from our measurements that the measured high-energy absorption in the  $\text{Ti:Al}_2\text{O}_3$  samples may not be associated with  $\text{Ti}^{3+}$  ions substituting in the  $\text{Al}^{3+}$  sites and may, in fact, be associated with some other defect.

Nath and Walda<sup>13</sup> reported that the addition of trace amounts of  $\text{TiO}_2$  ( $< 100$  parts in  $10^6$ ) had a substantial effect on the UV absorption edge of  $\text{Al}_2\text{O}_3$ , suggesting that the  $\text{Ti}^{4+}$  ion could be responsible for the observed UV absorption. Later experiments by Bessonova *et al.*<sup>14</sup> showed that Ti-doped samples having both the  ${}^2T_2 \rightarrow {}^2E$  and the 190-nm absorption bands would exhibit both an appreciable increase in the intensity of the UV band and a disappearance of the  ${}^2T_2 \rightarrow {}^2E$  band after annealing in oxygen at high temperatures. The authors concluded that  $\text{Ti}^{4+}$  ions were therefore responsible for the 190-nm band.

All the  $\text{Ti:Al}_2\text{O}_3$  crystals used for laser experiments exhibited an unexpectedly high loss at the laser wavelength. An investigation of the loss showed the existence of a broad, weak absorption band extending into the near infrared. Figure 4 plots the band for two polarizations at room temperature, observed from a Czochralski-grown crystal<sup>15</sup> doped (as determined by optical absorption measurements)

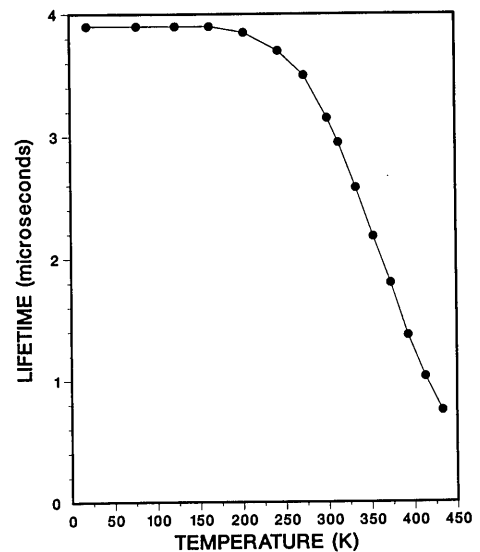


Fig. 3. Fluorescence lifetime versus temperature for the  ${}^2E \rightarrow {}^2T_2$  transition in  $\text{Ti:Al}_2\text{O}_3$ .

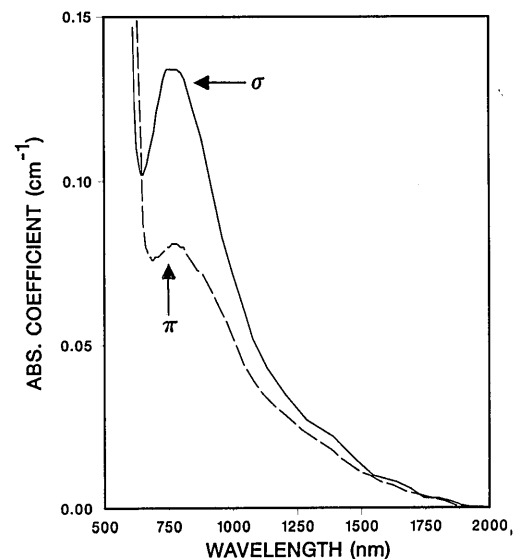


Fig. 4. Polarized measurement of the infrared absorption band in  $\text{Ti:Al}_2\text{O}_3$ .

with  $\sim 0.08$  wt. %  $\text{Ti}_2\text{O}_3$ . Note that in contrast to the  $\text{Ti}^{3+}$  absorption band in Fig. 1, the  $\sigma$  polarization is more intense than the  $\pi$  polarization. The intensity of the near-infrared absorption band was found to vary among samples having roughly the same  $\text{Ti}^{3+}$  doping level and decreased as the  $\text{Ti}^{3+}$  concentration decreased. From the limited number of samples examined we observed that material grown by the heat-exchanger method<sup>16</sup> had a lower level of absorption than Czochralski-grown crystals. The identification and elimination of the defect or defects responsible for the absorption band is currently an active research area. Two theories of the origin of the infrared absorption band have been proposed. One<sup>17</sup> associates the absorption with  $\text{Ti}^{3+}$  ions in interstitial or defect sites or at sites close to native defects. There is some evidence that postgrowth annealing can reduce the infrared band intensity.<sup>17</sup> The other<sup>18</sup> proposes that pairs of  $\text{Ti}^{3+}$ - $\text{Ti}^{4+}$  ions are responsible, based on observations of pair-related absorption in solutions.<sup>19</sup>

## GAIN MEASUREMENTS

Optical gain in  $\text{Ti:Al}_2\text{O}_3$  was measured by collinear propagation of focused,  $\text{TEM}_{00}$ -mode pump and probe beams through a 0.9-cm-long crystal doped with  $\sim 0.1$  wt. %  $\text{Ti}_2\text{O}_3$ . The  $\pi$ -polarized probe beam was from a krypton-ion laser operating at 676.5 nm, while the pump beam was the 514.5-nm output of an argon-ion laser. The gain cross section at the probe-beam wavelength,  $\sigma_{pr}$ , was estimated by use of the following expression:

$$\sigma_{pr} = \frac{\pi(b^2 + 1)hcw_{pu}^2 G}{2\lambda_{pu} P_{pu} \tau} [1 - \exp(-\alpha_{pu}l)]^{-1}, \quad (1)$$

where  $\tau$  is the fluorescence lifetime,  $G$  is the measured fractional gain in the probe beam,  $\alpha_{pu}$  is the absorption coefficient for the pump beam,  $l$  is the crystal length,  $\lambda_{pu}$  is the pump wavelength, and  $P_{pu}$  is the pump power in the crystal at the entrance surface. The quantity  $b$  is the ratio of the probe beam radius to that,  $w_{pu}$ , of the pump beam, while  $h$  and  $c$  are Planck's constant and the speed of light, respectively. For the experiment considered  $b$  was approximately 0.5,  $w_{pu}$  was  $6 \times 10^{-3}$  cm, and  $\alpha_{pu}$  was  $2.7 \text{ cm}^{-1}$ . A gain of  $1 \times 10^{-2}$  per watt of pump power was observed, leading to a calculated  $\sigma_{pr}$  of  $\sim 6.8 \times 10^{-20} \text{ cm}^2$ . Given the uncertainties in some of the measured quantities, especially the values for  $G$  and  $w_{pu}$ , the accuracy of  $\sigma_{pr}$  as determined by Eq. (1) is estimated to be  $\pm 30\%$ .

Figure 2 includes a curve for the gain cross-section line shape calculated using the relation between fluorescence and cross-section line shapes discussed in Appendix A. The broadening and extension to longer wavelengths of the gain line shape compared with the fluorescence line shape is especially noticeable for the large-linewidth  $\text{Ti:Al}_2\text{O}_3$  system. From the curve in Fig. 2 one predicts that the peak gain cross section is approximately four times the quantity  $\sigma_{pr}$ , and thus, based on the gain measurements, the peak gain cross section is  $\sim 2.7 \times 10^{-19} \text{ cm}^2$ .

The relation between spontaneous lifetime and gain cross section for uniaxial crystals, discussed in Appendix A, can be used to obtain an independent estimate of the peak gain cross section. The line shapes for  $\pi$ - and  $\sigma$ -polarized emission in Fig. 2 were numerically integrated, following Eq. (A9) in Appendix A, and used with Eq. (A8) to find a peak 300-K

gain cross section, at 795 nm, of  $\sim 4.8 \times 10^{-19} \text{ cm}^2$ , assuming a radiative lifetime of 3.15  $\mu\text{sec}$ . If the radiative lifetime is really (from Fig. 3) the low-temperature value of 3.87  $\mu\text{sec}$ , then the room-temperature fluorescence quantum efficiency is 0.81 and the peak gain cross section is  $3.9 \times 10^{-19} \text{ cm}^2$ . The discrepancy in cross sections between the pump-probe measurement and the derivation from lifetime could be resolved by assuming a lower value for the room-temperature quantum efficiency.

A test of the data on emission cross sections can be performed by comparing the integrated cross section for emission with that for absorption. The validity of the test relies on the use of the Condon approximation in treating the coupled system composed of the  $\text{Ti}^{3+}$  electron and the host crystal phonons. In that approximation, the electric-dipole matrix element between two levels of the coupled system is expressed as the product of an electric-dipole matrix element between the purely electronic part of the system wave function and an overlap integral between the initial and final phonon states. The dipole matrix element is assumed independent of the particular phonon states involved. Thus the oscillator strengths for absorption and emission are equal, when degeneracies are properly accounted for. Using the oscillator-strength formula given in Appendix A we calculated for absorption an oscillator strength of  $1.94 \times 10^{-4}$ , based on the data in Fig. 1 and on degeneracies of 3 and 2 in the initial and final states, respectively. In the calculation of the emission oscillator strength we assume that the emission is effectively from only one of the  ${}^2E$  states, and thus the initial- and final-state degeneracies are 1 and 3, respectively. In that case the emission oscillator strength will equal that for absorption if the peak cross section is  $4.3 \times 10^{-19} \text{ cm}^2$ , in reasonable agreement with the values derived in the measurements above. If the Condon approximation holds we would conclude that the fluorescence quantum efficiency for  $\text{Ti:Al}_2\text{O}_3$  is close to unity.

## PULSED-LASER OPERATION

### Dye-Laser Pumping

Laser operation from  $\text{Ti:Al}_2\text{O}_3$  was first observed by longitudinally pumping the same crystal used in gain measurements with the 503-nm output of a coaxial flash-lamp-pumped Coumarin 504 dye laser. The 26-cm-long  $\text{Ti:Al}_2\text{O}_3$ -laser cavity consisted of an 8%-transmission flat mirror and a 15%-transmission, 75-cm-radius concave mirror. Figures 5(a), 5(b), and 5(c) show the pulse shapes of the pump laser and the  $\text{Ti:Al}_2\text{O}_3$  laser at two pump levels over threshold; relaxation oscillations in the  $\text{Ti:Al}_2\text{O}_3$  laser are evident. The uncoated crystal used was of poor optical quality, exhibiting considerable scattering and optical distortion, and an output energy of only 1 mJ could be observed at a pump energy of 36 mJ. The laser output wavelength was in the region 750–760 nm. As Fig. 2 indicates, one would have expected operation at a somewhat longer wavelength from the position of the peak in the gain cross section. The wavelength variation of absorption in the crystal around the laser operating region (an example for one crystal appears in Fig. 4) may have shifted the net gain to shorter wavelengths, however.

Higher-quality crystals were obtained subsequent to the

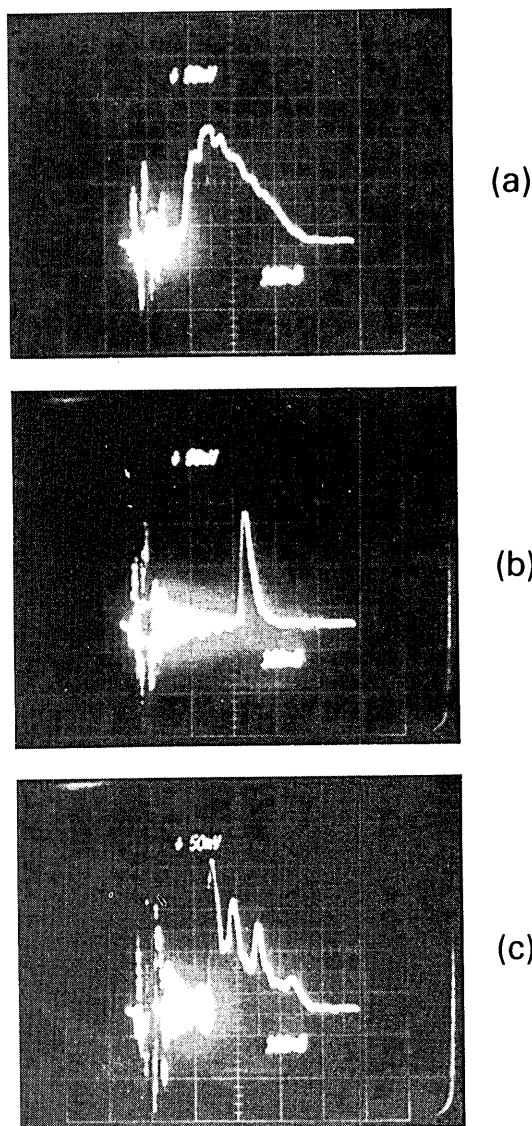


Fig. 5. Pump pulse shape (a) and Ti:Al<sub>2</sub>O<sub>3</sub> laser pulses at (b) 1.6-times threshold and (c) 3.6-times threshold. Time scale is 100 nsec per large division. Signals at left of traces are electrical noise.

initial laser demonstration. Two laser rods were fabricated from the crystals; both were polished with flat, parallel end faces and antireflection coated for 750 nm. One crystal (referred to as heavily doped) was 2.1 cm long and had a Ti<sup>3+</sup> doping level of 0.1%, while the other crystal (referred to as lightly doped) was 3.2 cm in length and had a doping level of 0.02%. The measured absorption coefficients at 750 nm for  $\pi$ -polarized light were  $\sim 0.04$  and  $\sim 0.006$  cm<sup>-1</sup> for the heavily and lightly doped crystals, respectively.

Absorption from the  ${}^2T_2 \rightarrow {}^2E$  transition in the heavily doped crystal was sufficiently intense to permit longitudinal pumping by the same coaxial flash-lamp-pumped dye laser used in the initial experiments, operating more efficiently with R6G dye at  $\sim 587$  nm. Figure 6 shows the output energy at  $\sim 750$  nm from the heavily doped crystal versus absorbed 587-nm pump energy for two different output-mirror transmissions. The optical cavity comprises a highly reflecting 25-cm-radius concave mirror and a flat output mirror, spaced 15 cm apart. Analysis of the data in Fig. 6

indicates that the slope quantum efficiency obtained with the 37%-transmission mirror was 67%. The internal loss in the laser can be calculated by two techniques, one based on the ratio of the thresholds for the two output mirrors (2.3) and the other based on the ratio of slope efficiencies (2.7). If  $L$  is the internal loss,  $T_1$  and  $T_2$  are two different output-mirror transmissions,  $R_{TH}$  is ratio of the threshold observed with  $T_2$  to that with  $T_1$ , and  $R_\Delta$  is the ratio of the slope efficiency observed with  $T_2$  to that with  $T_1$ , then

$$L = (T_2 - R_1 T_{TH}) / (R_{TH} - 1) \quad (2)$$

and

$$L = (R_\Delta - 1) T_1 T_2 / (T_2 - R_\Delta T_1). \quad (3)$$

The assumptions for these equations are that the threshold and slope efficiency are proportional to  $L + T_i$  and  $T_i / (T_i + L)$ , respectively, where  $i = 1$  or 2. We found the same value for  $L$  (18%) using both techniques; the value was in good agreement with the measured absorption coefficient of the laser crystal.

Tuning experiments on the dye-laser-pumped system were carried out by insertion of two Brewster-angle, fused-silica prisms into the laser cavity. (Experiments with a Littrow-mounted grating as the tuning element proved to be unreliable because of optical damage to the grating surface.) The cavity length was extended to  $\sim 25$  cm with the addition of the prisms, and the flat output mirror was replaced with another 25-cm-radius mirror. With a set of mirrors coated for operation at 750 nm, with 6% output coupling at that wavelength, laser operation over the wavelength range 687–821 nm was observed at an absorbed pump energy of  $\sim 8$  mJ. When the mirror set was changed to one coated for 850 nm, with 5% coupling, tuning from 726 to 986 nm was possible at the same pumping level. The short-wavelength tuning limit was extended to 660 nm by the use of a set of 632.8-nm He-Ne laser mirrors in the cavity along with the lightly doped laser crystal pumped at 503 nm.

Although laser operation was readily obtained by use of the dye-laser pump, the low repetition rate (1 Hz) of the

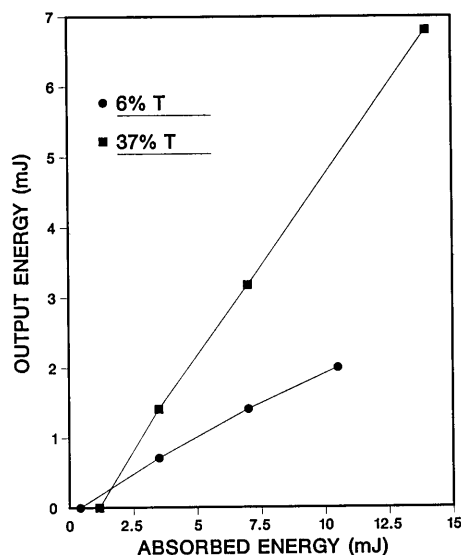


Fig. 6. Output energy versus absorbed pump energy with two different output-mirror transmissions for dye-laser-pumped Ti:Al<sub>2</sub>O<sub>3</sub> laser.

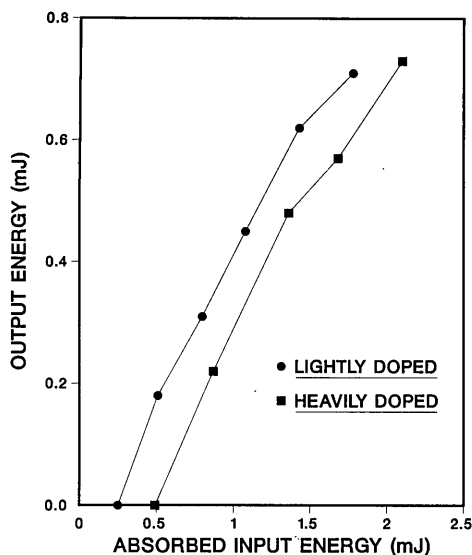


Fig. 7. Output energy versus absorbed input energy for two different laser crystals, pumped by a frequency-doubled Nd:YAG laser.

pump and the fluctuations in output energy and mode properties from one pulse to the next made characterization of some properties of the  $\text{Ti:Al}_2\text{O}_3$  laser difficult. Additional data, described in the following subsection, were taken on 532-nm, frequency-doubled Nd:YAG-laser-pumped systems.

#### Doubled Nd:YAG-Laser Pump

As for the case of dye-laser pumping, longitudinal excitation of the crystal (through one of the  $\text{Ti:Al}_2\text{O}_3$  laser-cavity mirrors) was used in the experiments. At 532 nm the lightly and heavily doped crystals absorbed  $\sim 70$  and  $\sim 96\%$  of the incident pump energy, respectively.

The initial pump system used was a conventional stable-resonator, multimode, flash-lamp-pumped and Q-switched Nd:YAG laser, the output of which was externally doubled by a KD\*P crystal. The system produced 532-nm energies of up to 5.5 mJ at a 10-Hz repetition rate. Figure 7 shows output versus absorbed pump energy for the two crystals in a 17-cm-long optical cavity composed of a 25-cm-radius highly reflecting mirror and a flat output mirror. The output mirror transmissions at 750 nm were 25 and 49% for the lightly and heavily doped crystals, respectively. The slope quantum efficiency was 68% over most of the operating range of the lightly doped crystal and 78% over the initial portion of the range for the heavily doped crystal, and operating wavelengths were in the 750–760-nm region. Heating effects were evident in the latter material at the highest input energies, manifested in a change in the mode structure of the  $\text{Ti:Al}_2\text{O}_3$  laser output, from  $\text{TEM}_{00}$ -mode operation at low input energies to highly multimode operation at the highest energies. Near-diffraction-limited output could be obtained at high energies, however, by a defocusing of the pump beam.

We took data on laser threshold and slope efficiency for both crystals using other output-mirror transmissions. As for the case with the dye-laser pump, the loss associated with the heavily doped crystal was found to be in reasonable agreement with the measured value of  $0.04 \text{ cm}^{-1}$ . A consistent loss value was not determined for the lightly doped

crystal. In particular, the slope efficiency calculated from the data of Fig. 7 would be associated with a loss coefficient of  $0.018 \text{ cm}^{-1}$ . On the other hand, a threshold comparison between operation with 1 and 6% output couplings indicated a coefficient of  $0.008 \text{ cm}^{-1}$ , in close agreement with the measured absorption coefficient. The high loss derived from the slope efficiency could be related to an incomplete spatial overlap between the pump beam and the  $\text{Ti:Al}_2\text{O}_3$  cavity modes in the crystal owing to the divergence of the focused pump away from the focal point. Such an incomplete overlap would reduce laser efficiency and make the crystal losses appear to be higher than they actually were. Overlap effects are less of an issue with the heavily doped crystal because of the short ( $\sim 0.5 \text{ cm}$  to the  $1/e$  point) penetration depth of the pump radiation.

As part of the laser characterization, measurements of the pump-beam size at the crystal face were attempted by measuring pump transmission through a variety of calibrated apertures. Accurate results were difficult to obtain because the Q-switched pulse tended to ablate the aperture material, and if the beam intensity was attenuated to avoid ablation the transmitted power levels were difficult to measure. However, it was determined that 50- and 200- $\mu\text{m}$  apertures passed  $\sim 40$  and 90% of the pump energy, respectively. As was the case for dye-laser pumping, intracavity prisms were used to tune the output of the doubled-Nd:YAG-pumped laser. The same combinations of crystals and mirrors permitted tuning to be observed over the range 662–950 nm.

The temporal outputs of the  $\text{Ti:Al}_2\text{O}_3$  lasers were observed to consist of single pulses, characteristic of gain-switched operation resulting from a pump pulse width that was short compared with the upper-state lifetime of the pumped laser. The pump pulse width was  $\sim 20 \text{ nsec}$  full width at half-maximum (FWHM). The resulting  $\text{Ti:Al}_2\text{O}_3$  laser pulse widths ranged, with the laser systems characterized by Fig. 7, from 11 nsec FWHM for the lightly doped crystal pumped at  $\sim 2.5$  times threshold to the 5-nsec pulse shown in Fig. 8, observed from the heavily doped crystal pumped at  $\sim 5.5$  times threshold. The delay between the peak of the pump pulse and the peak of the  $\text{Ti:Al}_2\text{O}_3$  laser pulse varied, as

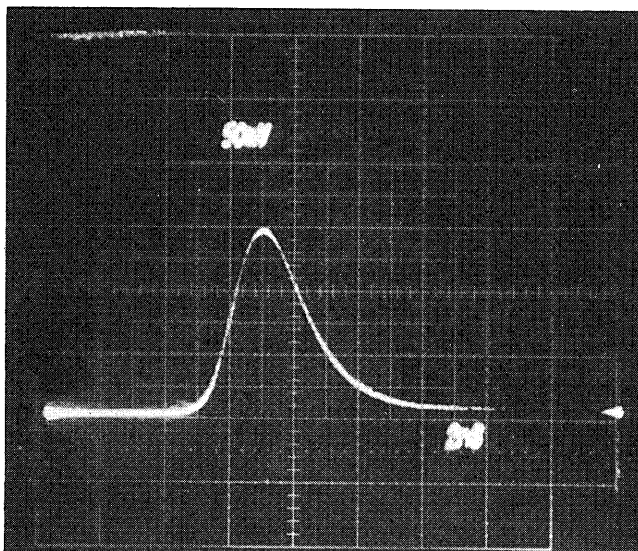


Fig. 8. Output pulse from a frequency-doubled Nd:YAG-pumped  $\text{Ti:Al}_2\text{O}_3$  laser. Time scale is 4 nsec per large division.

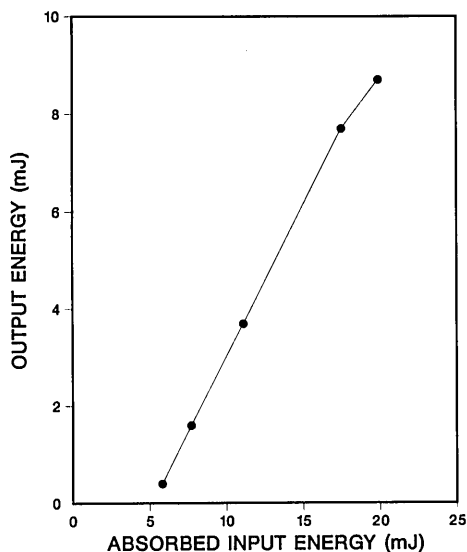


Fig. 9. Output energy versus absorbed input energy for a Ti:Al<sub>2</sub>O<sub>3</sub> laser pumped by an unstable-resonator, frequency-doubled Nd:YAG laser.

expected, with the pump ratio, from 45 nsec at 2.5 times threshold to 15 nsec at 6 times threshold. Computer models based on the standard rate-equation approach to laser dynamics (e.g., Ref. 20) confirmed that only a single pulse should be generated given the pump and Ti:Al<sub>2</sub>O<sub>3</sub> laser-cavity characteristics and that the buildup times and pulse widths observed experimentally were reasonable. For the particular data of Fig. 8 the computer-generated pulse width was 1 nsec instead of the observed 5. Some of this difference is due to the  $\sim 1$  nsec rise time of the detector-oscilloscope combination (a vacuum photodiode driving a Tektronix 7834 oscilloscope). The major cause of the discrepancy is likely the limitations of the rate-equation approach, the assumptions of which become invalid when the cavity round-trip time (1 nsec in this case) is an appreciable fraction of the predicted laser pulse width.

Considerably higher pump energies were obtained by employing an unstable-resonator configuration with the Nd:YAG pump laser; pulse energies at 532 nm of up to 45 mJ at a 10-Hz repetition rate were generated. Figure 9 presents output energy versus absorbed input energy for a Ti:Al<sub>2</sub>O<sub>3</sub> laser assembled using the lightly doped crystal in a 60-cm-long resonator, which was composed of a flat, 750-nm highly reflecting mirror and a 2-m-radius, 30%-transmitting output mirror. The laser crystal was located  $\sim 10$  cm from the output mirror and pumped through the flat mirror. This particular arrangement was employed to minimize optical damage to the coating on the flat. The pump-beam diameter at the crystal was estimated to be  $\sim 1$  mm.

The slope quantum efficiency in Fig. 9 is 86%. The actual pump energy available from the doubling crystal was 1.9 times greater than the absorbed energy owing to the incomplete absorption of the pump in the crystal and reflection losses in the system optics; the overall conversion efficiency from available pump energy to Ti:Al<sub>2</sub>O<sub>3</sub> output energy was 23%. As for the stable-resonator pump, the Ti:Al<sub>2</sub>O<sub>3</sub> output consisted of a single pulse, and at the maximum energy shown in Fig. 9 the output pulse width was 38 nsec. Computer calculations predicted a pulse width of 20 nsec. In

addition to shortcomings in the theory, discussed above, an additional reason for the longer observed pulse width may have been the multi-transverse-mode nature of the Ti:Al<sub>2</sub>O<sub>3</sub> laser output. Unlike the previous Ti:Al<sub>2</sub>O<sub>3</sub> lasers, the unstable-resonator-pumped system had an excited volume in the Ti:Al<sub>2</sub>O<sub>3</sub> crystal large enough to permit several transverse modes to oscillate. The existence of slightly different buildup times for the different modes has the effect of spreading out in time the gain-switched output pulse.

The limit to the output energy for the unstable-resonator-laser-pumped system was set by pump-induced optical damage to the flat cavity mirror; damage occurred at energies slightly higher than shown in Fig. 9. It is advisable in development of higher-energy Ti:Al<sub>2</sub>O<sub>3</sub> lasers pumped by Q-switched, frequency-doubled Nd:YAG lasers to use pumping techniques that avoid passing the pump beam through one of the cavity mirrors.

### Argon-Ion-Laser Pumping

Quasi-cw operation was obtained from the Ti:Al<sub>2</sub>O<sub>3</sub> laser by use of an argon-ion laser as a pump source. The argon-ion laser, operating on all lines in the blue-green wavelength region, was focused by a 17-cm-focal-length lens through a 25-cm-radius mirror (having 100% reflectivity at 750 nm) into the lightly doped Ti:Al<sub>2</sub>O<sub>3</sub> crystal. The laser cavity was completed by another 25-cm-radius mirror having  $\sim 1\%$  transmission at 750 nm, spaced 30 cm from the highly reflecting mirror. The laser crystal, in the center of the cavity, was attached to a copper heat sink and placed in a vacuum, along with the two cavity mirrors, to allow operation either with the crystal at room temperature or with the heat sink cooled to  $\sim 80$  K by liquid nitrogen. Under the latter conditions operation was obtained at a pump power (peak) of 4.8 W incident on the laser crystal. Heating effects were evident in the sensitivity of optimum mirror alignment to pump power above threshold and were reduced by mechanically chopping the pump beam such that the pump was on only 16% of the time. With the liquid-nitrogen cooling a peak output power from the Ti:Al<sub>2</sub>O<sub>3</sub> laser of 150 mW was obtained at an incident pump power of 7.4 W. Laser output was in the TEM<sub>00</sub> mode. The slope quantum efficiency was  $\sim 11\%$  based on a measured absorbed/incident pump-power ratio of 0.73. Quasi-cw operation was also observed with the crystal at room temperature, with a threshold incident peak pump power of 5.6 W. Heating effects were much more evident at room temperature because of the lower thermal conductivity of Al<sub>2</sub>O<sub>3</sub> compared with that at liquid-nitrogen temperatures. Fluctuations in the output power on a 200- $\mu$ sec time scale were evident during a 1.6-msec-long pump pulse, and a peak power output of only  $\sim 45$  mW could be obtained at a pump level of  $\sim 7$  W. Some effects on laser operation of the reduction in upper-state lifetime with temperature, evident in Fig. 3, were likely for the room-temperature Ti:Al<sub>2</sub>O<sub>3</sub> laser.

A theory developed for longitudinally pumped lasers<sup>20</sup> operating in the TEM<sub>00</sub> mode and pumped by a TEM<sub>00</sub>-mode laser is appropriate for the system discussed above. The threshold pump power,  $P_{TH}$ , is given by the expression

$$P_{TH} = \frac{\pi E_p w_L^2 (L + T) (a^2 + 1)}{4\sigma\tau [1 - \exp(-al)]}, \quad (4)$$

where  $E_p$  is the energy of a pump photon,  $w_L$  is the beam

radius of the laser cavity mode in the crystal,  $L$  is the laser internal loss,  $T$  is the output-mirror transmission,  $a$  is the ratio  $w_p/w_L$ , where  $w_p$  is the beam radius of the pump,  $\sigma$  is the peak gain cross section,  $\tau$  is the upper-state lifetime, and  $\alpha l$  is the product of the absorption coefficient for the pump and the crystal length. The appropriate values for the cw-pumping experiment were  $w_L = 1.7 \times 10^{-2}$  cm,  $w_p = 4 \times 10^{-3}$  cm,  $E_p \approx 4 \times 10^{-19}$  J, and  $1 - \exp(-\alpha l) = 0.73$ . The value used for  $L + T$  was 0.05, and the lifetime was 3.87  $\mu$ sec at 77 K and 3.15  $\mu$ sec at room temperature. The observed thresholds for liquid nitrogen and room temperature were consistent with gain cross sections of  $3.6 \times 10^{-19}$  and  $3.8 \times 10^{-19}$  cm<sup>2</sup>, respectively. Thus we find good agreement between the cross section calculated using the lifetime and fluorescence spectra and the cross section deduced from the cw-laser threshold. The slope efficiency was predicted to be 20% compared with the 11% observed, and there is, as yet, no good explanation for this discrepancy. In one experiment the transmission of pump power through the crystal at room temperature was measured as a function of incident power up to the 6-W level, in an effort to detect any unexpected saturation effects. The transmission was observed to be invariant, however.

## CONCLUSIONS

The laser performance of Ti:Al<sub>2</sub>O<sub>3</sub> is reasonably well understood based on the fundamental spectroscopic properties of the crystal. Laser operation spanning the entire expected gain linewidth and efficient, nearly quantum-limited conversion of pump energy have been observed. Such behavior is possible because the simple energy-level structure of the Ti<sup>3+</sup> ion does not permit excited-state absorption of either the pump or Ti:Al<sub>2</sub>O<sub>3</sub> laser radiation, provided that any charge-transfer transitions are sufficiently high in energy; this condition appears to be met in Ti:Al<sub>2</sub>O<sub>3</sub>. The short upper-state lifetime is anomalous for paramagnetic-ion systems based on parity-forbidden transitions and is the result of the strong trigonal field in the Al<sub>2</sub>O<sub>3</sub> host, which causes a significant deviation from an inversion-symmetry environment for the Ti<sup>3+</sup> ion. Fortunately, the short lifetime is accompanied by a relatively large (especially for tunable systems) peak gain cross section. Three independent techniques for determining the cross section yield values in the range  $(3-4) \times 10^{-19}$  cm<sup>2</sup>. The most significant improvement in the quality of existing Ti:Al<sub>2</sub>O<sub>3</sub> crystals would be a reduction in the as-yet-unidentified absorption in the laser wavelength region, an absorption not associated with isolated Ti<sup>3+</sup> ions. It is likely that laser operation from Ti<sup>3+</sup> in other host crystals can be obtained, and the search for new hosts should be an interesting challenge for both materials scientists and laser physicists.

## APPENDIX A

McCumber<sup>21</sup> defines a spontaneous emission function  $f_\zeta(\mathbf{k}, \nu)$  such that  $f_\zeta(\mathbf{k}, \nu)d\Omega_{\mathbf{k}\zeta}$  is the average intensity in photons/second for one of the two possible independent polarizations, per unit frequency interval of frequency  $\nu$  radiation emitted in the direction of the unit vector  $\mathbf{k}$  into the solid angle  $d\Omega_{\mathbf{k}\zeta}$ , from each excited fluorescent center. We have changed his notation to use  $\zeta$  as an index for one of the

polarizations and also use frequency  $\nu$  instead of angular frequency  $\omega$ . The gain cross section  $\sigma_\zeta(\mathbf{k}, \nu)$  is related to the spontaneous emission function by<sup>21</sup>

$$\sigma_\zeta(\mathbf{k}, \nu) = f_\zeta(\mathbf{k}, \nu)c^2/n^2\nu^2, \quad (\text{A1})$$

where  $n$  is the refractive index of the host crystal, approximated in this discussion as isotropic. We can define another spontaneous emission function,  $G_\zeta(\mathbf{k}, \lambda)$ , which is similar to  $f_\zeta(\mathbf{k}, \nu)$  but gives emission intensity in terms of more experimentally useful units, watts per unit wavelength interval, as a function of free-space wavelength  $\lambda = c/\nu$ . A straightforward calculation, accounting for the change in variables, allows the gain cross section as a function of wavelength to be expressed by

$$\sigma_\zeta(\mathbf{k}, \lambda) = \frac{\lambda^5 G_\zeta(\mathbf{k}, \lambda)}{hc^2n^2}. \quad (\text{A2})$$

This relation was used to calculate the gain cross-section line shape shown in Fig. 2.

For a uniaxial crystal such as Ti:Al<sub>2</sub>O<sub>3</sub> it is possible to derive the directional and polarization variation in spontaneous-emission intensity. We establish a spherical coordinate system for the direction of emission based on the angle  $\theta$  between  $\mathbf{k}$  and the  $c$  axis and the angle  $\phi$  between the projection of  $\mathbf{k}$  on a plane perpendicular to the  $c$  axis and some arbitrary axis in that plane. The orientation of the polarization (transverse to  $\mathbf{k}$ ) is measured by the angle  $\psi$ . For  $\psi = 0$  the polarization lies in the plane perpendicular to the  $c$  axis, the  $\sigma$  polarization. After some geometrical calculations one finds that the spontaneous-emission function can be expressed as

$$G(\lambda, \theta, \phi, \psi) = G_\sigma(\lambda)(\cos^2 \psi + \sin^2 \psi \cos^2 \theta) + G_\pi(\lambda)\sin^2 \psi \sin^2 \theta, \quad (\text{A3})$$

where  $G_\sigma(\lambda)$  and  $G_\pi(\lambda)$  are emission functions for purely  $\sigma$ - and  $\pi$ -polarized radiation, respectively. As expected, there is no variation in the function with  $\phi$ .

McCumber relates the spontaneous emission lifetime,  $\tau$ , to the emission function  $f_\zeta(\mathbf{k}, \nu)$  by the following:

$$1/\tau = \sum_{\zeta} \int_{4\pi} d\Omega_{\mathbf{k}\zeta} \int_0^\infty f_\zeta(\mathbf{k}, \nu)d\nu, \quad (\text{A4})$$

where the summation is to be made over two independent (i.e., orthogonal) polarizations. The lifetime can be related to the  $G(\lambda, \theta, \phi, \psi)$  function by

$$1/\tau = \frac{1}{hc} \int_\infty^0 d\lambda \int_0^{2\pi} d\phi \int_0^\pi d\theta \sin \theta [G_\zeta(\lambda)(1 + \cos^2 \theta) + G_\pi(\lambda)\sin^2 \theta], \quad (\text{A5})$$

where the sum has been taken over two linear polarizations, one with  $\psi = 0$  and the other with  $\psi = \pi/2$ . After carrying out the integrations over angle we are left with

$$1/\tau = \frac{8\pi}{hc} \int_\infty^0 [2/3 G_\sigma(\lambda) + 1/3 G_\pi(\lambda)]d\lambda. \quad (\text{A6})$$

It is possible given knowledge of the emission functions  $G_\sigma(\lambda)$  and  $G_\pi(\lambda)$  and the lifetime to determine the gain cross section. Experimental measurements of the functions typi-

cally determine them to within some multiplicative constant.

We define the experimentally measured functions

$$\begin{aligned} g_{\sigma}(\lambda) &= \alpha G_{\sigma}(\lambda), \\ g_{\pi}(\lambda) &= \alpha G_{\pi}(\lambda), \end{aligned} \quad (\text{A7})$$

where  $\alpha$  is a constant. By use of Eqs. (A2) and (A6) one can find the cross section in terms of the angular variables discussed above, such that

$$\begin{aligned} \sigma(\theta, \psi, \lambda) \\ = \frac{\lambda^5 [g_{\pi}(\lambda) \sin^2 \psi \sin^2 \theta + g_{\sigma}(\lambda) (\cos^2 \psi + \sin^2 \psi \cos^2 \theta)]}{8\pi c n^2 \tau I}, \end{aligned} \quad (\text{A8})$$

where

$$I = \int_{\infty}^0 [2/3 g_{\sigma}(\lambda) + 1/3 g_{\pi}(\lambda)] \lambda d\lambda. \quad (\text{A9})$$

If the measured spontaneous-emission lifetime results from a combination of radiative and nonradiative decay, then one can define a fluorescence quantum efficiency,  $\eta$ , as the ratio of the radiative rate to the total rate, where the total rate is the inverse of the measured lifetime. The cross section calculated in Eq. (A8) must be multiplied by  $\eta$  to derive the actual gain cross section.

Another important spectroscopic quantity is the oscillator strength of a transition. If  $F_{if}$  is the oscillator strength for a transition from initial level  $i$  to final level  $f$ , then, for a uniaxial crystal (in CGS units)

$$F_{if} = \frac{g_i m c^2}{g_f \pi e^2} \frac{9n}{(n^2 + 2)^2} \int_{\infty}^0 [2/3 \sigma_{\sigma}(\lambda) + 1/3 \sigma_{\pi}(\lambda)] \frac{d\lambda}{\lambda^2}, \quad (\text{A10})$$

where  $m$  and  $e$  are the mass and charge of the electron, respectively, and  $g_i$  and  $g_f$  are the degeneracies of the initial and final levels, respectively.  $\sigma_{\sigma}(\lambda)$  and  $\sigma_{\pi}(\lambda)$  are the cross sections for  $\sigma$ - and  $\pi$ -polarized emission, respectively. The derivation of the equation is based on the averaging techniques for uniaxial crystals discussed above and on the use of the Lorentz-Lorenz correction for the local field in the crystal, as discussed by Curie.<sup>22</sup>

## ACKNOWLEDGMENTS

The author gratefully acknowledges discussions on theory with H. J. Zieger and P. L. Kelley, the technical assistance of J. F. Bushee in the experimental work, and the work of E. Owens in x-ray analysis, all at Lincoln Laboratory. The crystal used in the gain measurements and first laser demonstration was provided by R. L. Coble of MIT. The two crystals used in later laser measurements were from boules grown at Crystal Systems by C. Khattak. The growth effort at Crystal Systems was supported by the National Science Foundation under grant DMR-8260712.

The author would also like to thank P. Lacovara of the Naval Research Laboratory for providing a preprint of Ref. 17.

The major portion of this work, including all the experiments, was performed at Lincoln Laboratory and was sponsored by the U.S. Department of the Air Force. Work at

Schwartz Electro-Optics was sponsored by the National Aeronautics and Space Administration.

## REFERENCES

1. Operation of the Ti:Al<sub>2</sub>O<sub>3</sub> laser was first reported by the author at the Twelfth International Quantum Electronics Conference in Munich in June 1982. Brief articles appeared in *Physics News in 1982*, P. F. Schewe, ed. (American Institute of Physics, New York, 1983) and in *Solid State Research Report* (Lincoln Laboratory, MIT, 1982:3), pp. 15–21. A more complete description of the author's efforts was in the chapter "Recent advances in transition-metal-doped lasers," in *Tunable Solid State Lasers*, Springer Series in Optical Sciences, P. Hammerling, A. Budgor, and A. Pinto, eds. (Springer-Verlag, Berlin, 1985), pp. 4–10. Work by others includes P. Lacovara, L. Esterowitz, and R. Allen, "Flash-lamp pumped Ti:Al<sub>2</sub>O<sub>3</sub> laser using fluorescent conversion," *Opt. Lett.* **10**, 273–275 (1985); G. F. Albrecht, J. M. Eggleston, and J. J. Ewing, "Measurements of Ti<sup>3+</sup>:Al<sub>2</sub>O<sub>3</sub> as a lasing material," *Opt. Commun.* **52**, 401–404 (1985); B. K. Sevast'yanov *et al.*, "Tunable laser based on Al<sub>2</sub>O<sub>3</sub>:Ti<sup>3+</sup> crystal," *Sov. Phys. Crystallog.* **29**, 566–567 (1984).
2. E. D. Nelson, J. Y. Wong, and A. L. Schawlow, "Far infrared spectra of Al<sub>2</sub>O<sub>3</sub>:Cr<sup>3+</sup> and Al<sub>2</sub>O<sub>3</sub>:Ti<sup>3+</sup>," *Phys. Rev.* **156**, 298–308 (1967).
3. R. R. Joyce and P. L. Richards, "Far infrared spectra of Al<sub>2</sub>O<sub>3</sub> Doped with Ti, V and Cr," *Phys. Rev.* **179**, 375–380 (1969).
4. R. M. MacFarlane, J. Y. Wong, and M. D. Sturge, "Dynamic Jahn-Teller effect in octahedrally coordinated d<sup>1</sup> impurity systems," *Phys. Rev.* **166**, 250–258 (1968).
5. D. S. McClure, "Optical spectra of transition-metal ions in corundum," *J. Chem. Phys.* **36**, 2757–2779 (1962).
6. T. P. Jones, R. L. Coble, and C. J. Mogab, "Defect diffusion in single crystal aluminum oxide," *J. Am. Ceram. Soc.* **52**, 331–334 (1969).
7. G. A. Keig, "Influence of the valence state of added impurity ions on the observed color in doped aluminum oxide single crystals," *J. Cryst. Growth* **2**, 356–360 (1968).
8. H. K. Eigenmann, Ph.D. dissertation (Swiss Federal Institute of Technology, Zurich, Switzerland, 1970).
9. B. F. Gachter and J. A. Koningstein, "Zero phonon transitions and interacting Jahn-Teller phonon energies from the fluorescence spectrum of  $\alpha$ -Al<sub>2</sub>O<sub>3</sub>:Ti<sup>3+</sup>," *J. Chem. Phys.* **60**, 2003–2006 (1974).
10. Similar results have been observed by K. L. Schepler, AFAL, Wright-Patterson Air Force Base, Ohio 45433 (personal communication, 1983).
11. Similar fluorescence lifetime data have been observed by G. Huber, University of Hamburg, Hamburg, Federal Republic of Germany (personal communication, 1984).
12. H. H. Tippins, "Charge-transfer spectra of transition-metal ions in corundum," *Phys. Rev. B* **1**, 126–135 (1970).
13. G. Nath and G. Walda, "Strong reduction of laser produced damage in sapphire and ruby by doping with TiO<sub>2</sub>," *Z. Naturforsch.* **A23**, 624–625 (1968).
14. T. S. Bessonova, M. P. Stanislavskii, and V. Ya. Khaimov-Malkov, "Effect of heat treatment and irradiation on absorption spectra of Ti and Si corundum," *Opt. Spectrosc. (USSR)* **41**, 87–88 (1976).
15. Electronics Division, Union Carbide, San Diego, Calif.
16. Crystal Systems, Inc., Salem, Mass.
17. P. Lacovara, L. Esterowitz, and M. Kokta, "Growth, spectroscopy and lasing of titanium-doped sapphire," *IEEE J. Quantum Electron.* **QE-21**, 1614–1618 (1985).
18. C. K. Jorgenson, University of Geneva, Geneva, Switzerland (personal communication, 1985).
19. C. K. Jorgenson, "Comparative ligand field studies IV," *Acta Chem. Scand.* **11**, 73–85 (1957).
20. P. F. Moulton, "An investigation of the Co:MgF<sub>2</sub> laser system," *IEEE J. Quantum Electron.* **QE-21**, 1582–1595 (1985).
21. D. E. McCumber, "Theory of phonon-terminated optical masters," *Phys. Rev.* **134**, A299–A306 (1964).
22. D. Curie, *Luminescence in Crystals* (Methuen, London, 1963), p. 69.

## P. F. Moulton



P. F. Moulton was born in Springfield, Massachusetts, on May 27, 1946. He received the A.B. degree in physics from Harvard University, Cambridge, Massachusetts, in 1968 and the M.S. and Ph.D. degrees from the Department of Electrical Engineering and Computer Science, Massachusetts Institute of Technology, Cambridge, in 1971 and 1975, respectively. He spent a postdoctorate year in 1975 at MIT Lincoln Laboratory, Lexington, Massachusetts, and became a staff member there in 1976. His work at

Lincoln Laboratory included high-resolution infrared spectroscopic measurements of molecules, development of lasers for remote sensing, and research and development of tunable and high-efficiency solid-state lasers. Since 1985 he has been Vice-President and General Manager of the Boston Division of Schwartz Electro-Optics, Concord, Massachusetts, where he is engaged in the research and development of a variety of solid-state laser systems. Dr. Moulton is a senior member of the Institute of Electrical and Electronics Engineers and a member of the Optical Society of America.